Non-Unit DC Line Protection Method for Multi-Terminal MMC-HVDC System Based on Normalized Backward Traveling Waves

Xie, Fan; Liu, Le; Hao, Zhiguo; Lekić, Aleksandra; Popov, Marjan

DOI
10.1109/ISGTEUROPE56780.2023.10408224

Publication date
2023

Document Version
Final published version

Published in
Proceedings of 2023 IEEE PES Innovative Smart Grid Technologies Europe, ISGT EUROPE 2023

2023 IEEE PES Innovative Smart Grid Technologies Europe (ISGT EUROPE) | 979-8-3503-9678-2/23/$31.00 ©2023 IEEE | DOI: 10.1109/ISGTEUROPE56780.2023.10408224

Non-Unit DC Line Protection Method for Multi-Terminal MMC-HVDC System Based on Normalized Backward Traveling Waves

Fan Xie[1,2*], Le Liu[2], Zhiguo Hao[1], Aleksandra Lekić[2], and Marjan Popov[2]
[1]*School of Electrical Engineering, Xi'an Jiaotong University, Xi'an, China*
[2]*Faculty of Electrical Engineering, Mathematics & Computer Science, Delft University of Technology, Delft, The Netherlands*
xiefan_ee@stu.xjtu.edu.cn, {L.Liu-7, A.Lekic, M.Popov}@tudelft.nl, zhghao@mail.xjtu.edu.cn

***Abstract*—Existing line protection methods for multi-terminal direct current (MTDC) systems are constrained by the placement and values of boundary elements. To overcome this limitation, this paper proposes a non-unit DC line protection method based on the normalized backward traveling waves (BTWs) of the 1-mode voltage. Firstly, this article studies the traveling wave characteristics and derives the expressions for the normalized BTWs. Then, the Levenberg-Marquardt algorithm is used for amplitude fitting and normalization calculation. Based on the normalized BTWs, a non-unit protection method is proposed. Finally, the proposed method is evaluated with a simulation model on the PSCAD/EMTDC platform. The results demonstrate that the proposed method can accurately identify faults of different resistances and distances without requiring boundary devices, and is robust against noise disturbances (35 dB).**

***Index Terms*—Multi-terminal DC grid, Modular multilevel converter, Non-unit protection, Traveling wave, Levenberg-Marquardt algorithm.**

I. Introduction

MODULAR multilevel converter (MMC)-based HVDC technology has the benefits of independent active and reactive power control, flexible and adjustable power flow, and no commutation failure [1], [2]. Hence, it is suitable for constructing multi-terminal DC (MTDC) grids and has been proven to be a successful solution for the integration of renewable energy into the power system. Due to the lack of inertia in MTDC, fault currents will increase and propagate rapidly, endangering the security of power electronics [3]. Therefore, fast and reliable line protection is crucial for the operation of the systems [4].

DC protection includes unit and non-unit protection. The former uses multi-terminal electrical quantities, requiring long-distance signal communication and precise synchronisation [5]. The latter, which can escape the aforementioned requirements and speed up fault identification by using only local measurement, is the focus of this work. Currently, the non-unit line protections for the MTDC systems mainly concentrate on the differences between internal and external faults in the time domain or frequency domain caused by boundary devices, e.g., the smoothing reactors and DC filters [6].

The protection methods based on frequency-domain characteristics mostly use algorithms such as fast Fourier transform, wavelet transform (WT), and empirical modal decomposition to analyze and extract the energy distribution in different frequency bands. In [7], wavelet filters separate the DC current into detailed coefficients, representing the frequency-domain difference between internal and external faults. In [8], the Mallat algorithm processes voltage to produce detail coefficients at the selected level, then the peak energy of high-frequency transient voltage is computed to identify faults. In [9], the amplitudes of high-frequency voltage traveling waves (TWs) are compared between internal and external faults, and the WT modulus maximum is utilized to quantify the fault characteristic. However, these methods are generally constrained by the placement and values of the boundary devices, and they are vulnerable to high-frequency noise.

The protection methods based on time-domain characteristics mostly use differential and integral calculations to determine numerical characteristics, such as the rate of change of voltage (ROCOV) and the ratio of transient voltage (ROTV). The reactor serves as the boundary of the DC lines and offers the high-frequency component for a high-impedance channel, resulting in a clear difference between the reactor's ROTV during internal and external faults [10]. As analyzed in [11], the reactor power discontinues at the boundary devices and distinguishes significantly between internal and external faults. Therefore, a protection method is proposed based on this feature. In [12], a hybrid detection strategy is proposed. After the sensor measurements of line currents and reactor voltages, a learning algorithm chooses the optimal fault detector from a detector pool. However, these methods also rely on boundary devices due to energy distribution differences in the frequency domain. Furthermore, the threshold settings generally depend on numerical simulations, and the sensitivity is insufficient for faults with transient resistance.

This work presents a non-unit DC line protection method

This work was sponsored by the Key Research and Development Program of Shaanxi Province (No.2022GXLH-01-06) and the China Scholarship Council (No.202206280073).

based on the normalized BTWs of 1-mode voltage for MTDC systems to address the aforementioned issues. It has been verified that the proposed method can accurately identify various faults in a system without boundary devices. Furthermore, its performance is unaffected by fault resistance, and thresholds are chosen using analytical calculations.

II. Fault Analysis for the MTDC System

A. Configuration of the MTDC System

Fig.1 depicts the configuration of the four-terminal MMC-HVDC system, which is benchmarked by the Cigre B4.57 working group. The rated DC voltage is ±320 kV. The MMCs utilize half-bridge sub-modules (SMs) and are interconnected by cables with a protective relay (R) and a DC circuit breaker (CB) installed at both terminals [13]. For each MMC, the number of submodules (SMs) is 200, the SM capacitor is 15 mF, and the bridge arm inductance and resistance are 5 mH and 0.5 Ω, respectively. The rated capacity of each MMC is 1000 MVA, and the length of each cable is 200 km.

The $\mathrm{Cable_{MN}}$ is the studied cable in this work. As such, fault F1 is an internal fault for $\mathrm{R_{MN1}}$ and $\mathrm{R_{MN2}}$, while faults F2, F3, and F4 are external faults. Notably, no boundary devices, such as smoothing reactors, are installed at the cable terminal, unlike in typical MMC-based HVDC systems.

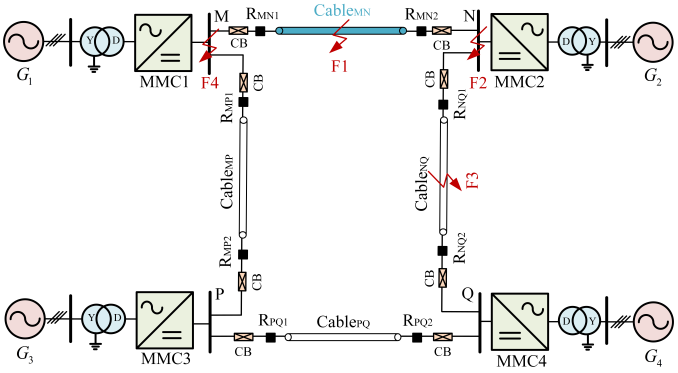

Fig. 1. The configuration of the four-terminal MMC-HVDC system.

B. Fault Analysis Under Internal Faults

The forward traveling waves (FTWs) and BTWs form the voltage and current along the cable, and because the initial BTWs are not refracted or reflected, they can represent the original TWs from the fault point. In addition, the electrical quantities in this work are transformed to 1-mode and 0-mode as follows, for eliminating the coupling between the poles [14]:

$$\begin{bmatrix} U_0 \\ U_1 \end{bmatrix} = \frac{1}{\sqrt{2}} \begin{bmatrix} 1 & 1 \\ 1 & -1 \end{bmatrix} \begin{bmatrix} U_\mathrm{P} \\ U_\mathrm{N} \end{bmatrix}, \begin{bmatrix} I_0 \\ I_1 \end{bmatrix} = \frac{1}{\sqrt{2}} \begin{bmatrix} 1 & 1 \\ 1 & -1 \end{bmatrix} \begin{bmatrix} I_\mathrm{P} \\ I_\mathrm{N} \end{bmatrix} \tag{1}$$

where the subscript P/N denotes poles, and 1/0 denote modes.

In case of F1, the S-domain expression for the 1-mode voltage BTWs $U_{\mathrm{b1,int}}$ measured in $\mathrm{R_{MN1}}$ is:

$$U_{\mathrm{b1,int}}(s,l) = \frac{U_{\mathrm{F1}}}{s} e^{-\gamma(s)\cdot l} \approx \frac{U_{\mathrm{F1}}}{s} \frac{1-kl}{1+s\cdot\tau l} e^{-s\cdot\frac{l}{v_1}}, \tag{2}$$

where l denotes the fault distance, and $e^{-\gamma(s)\cdot l}$ is the propagation function. For easy transformation to time domain, $e^{-\gamma(s)\cdot l}$ is further approximated [15]. Index k denotes the amplitude attenuation per unit length, and τ denotes the waveform distortion per unit length. U_{F1} is the initial values of the 1-mode TWs at the fault point. For a typical positive-pole-to-ground (PPTG) fault, negative-pole-to-ground (NPTG) fault, and pole-to-pole (PTP), the U_{F1} is determined by [16]:

$$\begin{cases} \text{PTP: } U_{\mathrm{F1}} = \dfrac{-\sqrt{2}Z_{\mathrm{C1}}U_\mathrm{r}}{Z_{\mathrm{C1}}+R_\mathrm{f}}, \\ \text{PPTG/NPTG: } U_{\mathrm{F1}} = \dfrac{-\sqrt{2}Z_{\mathrm{C1}}U_\mathrm{r}}{Z_{\mathrm{C1}}+Z_{\mathrm{C0}}+4R_\mathrm{f}}, \end{cases} \tag{3}$$

where U_r denotes the DC rated voltage, R_f denotes the fault resistance, and Z_C denotes the characteristic impedance.

The expression for $U_{\mathrm{b1,int}}$ in (2) can be rewritten as:

$$U_{\mathrm{b1,int}}(s,l) = A_{\mathrm{int}} \left(\frac{1}{s} - \frac{1}{s+1/\tau l} \right) e^{-s\cdot l/v_1}, \tag{4}$$

where $A_{\mathrm{int}} = u_{\mathrm{F1}}(1-kl)$ and v_1 denotes the 1-mode TWs velocity.

Using the inverse *Laplace* transform, we have the time-domain expression for $U_{\mathrm{b1,int}}$ as:

$$u_{\mathrm{b1,int}}(t,l) = A_{\mathrm{int}} \left(1 - e^{-(t-l/v_1)/\tau l} \right). \tag{5}$$

In (5), if fault F1 occurs, $u_{\mathrm{b1,int}}$ will have two components: step waves and exponential waves. Among these components, the amplitude of $u_{\mathrm{b1,int}}$ is determined by the step waves, and the exponential waves will attenuate to zero. To eliminate the impact of the R_f, $u_{\mathrm{b1,int}}$ can be further normalized as the normalized 1-mode voltage BTWs $u^*_{\mathrm{b1,int}}$:

$$u^*_{\mathrm{b1,int}}(t,l) = \frac{u_{\mathrm{b1,int}}(t,l)}{A_{\mathrm{int}}} = 1 - e^{-(t-l/v_1)/\tau l}, \tag{6}$$

Furthermore, the derivative of $u^*_{\mathrm{b1,int}}$ can be obtained as,

$$\frac{\mathrm{d}u^*_{\mathrm{b1,int}}(t,l)}{\mathrm{d}l} = -\frac{e^{-(t-l/v_1)/\tau l}}{\tau l^2} < 0, \tag{7}$$

As proven in (7), $u^*_{\mathrm{b1,int}}$ decreases while l increases.

C. Fault Analysis Under External Faults

In the case of F2, the 1-mode voltage BTWs $u_{\mathrm{b1,ext}}$ are the same as $u_{\mathrm{b1,int}}$ of F1, which occurs at the end of the protected cable because their faulty circuits are the same when neglecting CB impedance. In contrast, when F4 occurs in the opposite direction, only FTWs are injected into the protected cable, and the $u_{\mathrm{b1,ext}}$ stays at zero until the reflected waves reach from the other end.

According to Fig.2, the $U_{\mathrm{b1,ext}}$ measured in $\mathrm{R_{MN1}}$ under external fault F3 can be expressed in the S domain as follows:

$$\begin{aligned} U_{\mathrm{b1,ext}}(s,l') &= \frac{2U_{\mathrm{F1}}}{s} \frac{Z_{\mathrm{MMC}} \parallel Z_{\mathrm{C1}}}{Z_{\mathrm{C1}} + Z_{\mathrm{MMC}} \parallel Z_{\mathrm{C1}}} e^{-\gamma(s)\cdot l'} \\ &= \frac{U_{\mathrm{F1}}}{s} e^{-\gamma(s)\cdot l'} - \frac{U_{\mathrm{F1}}}{s} \frac{Z_{\mathrm{C1}} - Z_{\mathrm{MMC}} \parallel Z_{\mathrm{C1}}}{Z_{\mathrm{C1}} + Z_{\mathrm{MMC}} \parallel Z_{\mathrm{C1}}} e^{-\gamma(s)\cdot l'}, \end{aligned} \tag{8}$$

where l' denotes the fault distance, and Z_{MMC} denotes the equivalent impedance of MMC, which contains equivalent resistance R_{eq}, inductance L_{eq} and capacitance C_{eq} [17], as shown in Fig. 2(b).

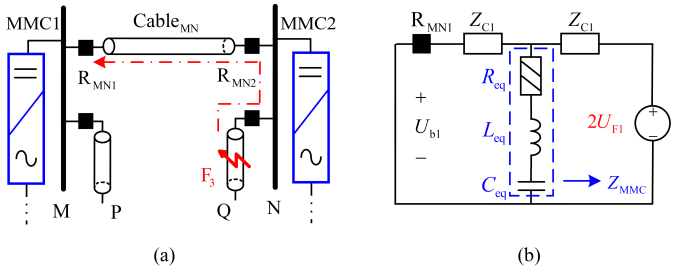

Fig. 2. The system model and faulty circuit when F3 occurs. (a) System model; (b) Faulty circuit.

Comparing (2) with (8), it is found that $U_{\mathrm{b1,ext}}$ contains the similar equations as $U_{\mathrm{b1,int}}$. Therefore, (8) is rewritten as:

$$U_{\mathrm{b1,ext}}(s,l') = U_{\mathrm{b1,int}}(s,l') - U_{\mathrm{b1,add}}(s,l'), \tag{9}$$

where $U_{\mathrm{b1,int}}(s,l')$ is $U_{\mathrm{b1,int}}$ of F1 with a fault distance l', and $U_{\mathrm{b1,add}}$ is the difference between $U_{\mathrm{b1,ext}}$ and $U_{\mathrm{b1,int}}$.

Substituting the expression for Z_{MMC} and the approximation of $e^{-\gamma(s)\cdot l'}$, we have $U_{\mathrm{b1,add}}$ as:

$$\begin{aligned} &U_{\mathrm{b1,add}}(s,l') \\ &\approx \frac{U_{\mathrm{F1}}}{s}\frac{Z_{\mathrm{C1}}}{Z_{\mathrm{C1}}+2(sL_{\mathrm{eq}}+R_{\mathrm{eq}}+1/sC_{\mathrm{eq}})}\frac{1-kl'}{1+s\cdot\tau l'}e^{-s\cdot\frac{l'}{v_1}}, \end{aligned} \tag{10}$$

The expression for $U_{\mathrm{b1,ext}}$ in (10) can be rewritten as:

$$U_{\mathrm{b1,add}}(s,l') = \left(\frac{A_1}{s-s_1}+\frac{A_2}{s-s_2}+\frac{A_3}{s+1/\tau l'}\right)e^{-s\cdot\frac{l'}{v_1}}, \tag{11}$$

where A_1, A_2, and A_3 are the numerators of rational fractions, s_1 and s_2 are the poles.

Substituting (4) and (11) into (9), we obtain $U_{\mathrm{b1,ext}}$ as:

$$U_{\mathrm{b1,ext}}(s,l') = \left(\frac{A_{\mathrm{ext}}}{s}-\frac{A_{\mathrm{ext}}+A_3}{s+\frac{1}{\tau_{\mathrm{ext}}}}-\frac{A_1}{s-s_1}-\frac{A_2}{s-s_2}\right)e^{-s\cdot T_{\mathrm{d}}}, \tag{12}$$

where $A_{\mathrm{ext}} = u_{\mathrm{F1}}(1-kl')$, $\tau_{\mathrm{ext}} = \tau l'$, and $T_{\mathrm{d}} = l'/v_1$.

Using the inverse *Laplace* transform, we have the time-domain expression for $U_{\mathrm{b1,ext}}$:

$$u_{\mathrm{b1,ext}}(t,l') = A_{\mathrm{ext}} - (A_{\mathrm{ext}}+A_3)e^{-\frac{t'}{\tau_{\mathrm{ext}}}} - A_1e^{s_1t'} - A_2e^{s_2t'}, \tag{13}$$

where $t' = t - T_{\mathrm{d}}$.

Comparing (4) and (12), we have that A_{int} equals A_{ext}, when fault distances are the same. This is because Z_{MMC} merely modifies the exponential waves of u_{b1} but not step waves, which determine A_{int} and A_{ext}. Hence, according to (9) and (7), the inequality relationship can be obtained as:

$$u^*_{\mathrm{b1,ext}}(t,l') < u^*_{\mathrm{b1,int}}(t,l') < u^*_{\mathrm{b1,int}}(t,l_{\mathrm{c}}), \tag{14}$$

where l_{c} denotes the length of the protected cable.

As shown in (14), $u^*_{\mathrm{b1,ext}}$ of F3 are constantly smaller than $u^*_{\mathrm{b1,int}}$ of F1 occurring at the end of the protected cable. In case of external faults, the $u^*_{\mathrm{b1,ext}}$ can be summarized with:

$$\begin{cases} \mathrm{F2}: & u^*_{\mathrm{b1,ext}}(t,l_{\mathrm{c}}) = u^*_{\mathrm{b1,int}}(t,l_{\mathrm{c}}) \\ \mathrm{F3}: & u^*_{\mathrm{b1,ext}}(t,l') < u^*_{\mathrm{b1,int}}(t,l_{\mathrm{c}}) \\ \mathrm{F4}: & u^*_{\mathrm{b1,ext}}(t,0) = 0 \end{cases} \tag{15}$$

According to (15), the $u^*_{\mathrm{b1,ext}}$ under external faults F2, F3, F4 are smaller than $u^*_{\mathrm{b1,int}}$ of internal fault F1. As such, this feature could be used to identify the faulty zone.

III. Non-Unit Protection Method Based on Normalised Backward Traveling Waves

A. Levenberg-Marquardt Algorithm

Voltage BTWs u_{b1} can be first obtained from the 1-mode voltage u_1 and current i_1 as,

$$u_{\mathrm{b1}}(t) = \frac{u_1(t) - Z_{\mathrm{C1}}(t)i_1(t)}{2}. \tag{16}$$

Then, to calculate u^*_{b1}, the amplitude A is identified using the L-M algorithm [18], of which the error function $\boldsymbol{F}(\boldsymbol{x})$ is defined as:

$$\boldsymbol{F}(\boldsymbol{x}) = \boldsymbol{F}(A,\tau) = u_{\mathrm{b1}}(t) - A\left(1-e^{-t/\tau}\right), \tag{17}$$

Based on (5) and (13), different formulations of $\boldsymbol{F}(\boldsymbol{x})$ should be utilized for $u_{\mathrm{b1,int}}$ and $u_{\mathrm{b1,ext}}$ due to different numbers of exponential terms. Nevertheless, in practice, only one $\boldsymbol{F}(\boldsymbol{x})$ is utilized since the fault type cannot be identified in advance. Additionally, the computation of u^*_{b1} is unaffected since the simplification only impacts the fit of τ (but not the fit of A).

The iteration goal is to find the optimal solution $\boldsymbol{x}_k$ that minimizes $\|\boldsymbol{F}(\boldsymbol{x})\|^2$. At each iteration k, the extended Jacobi matrix $\boldsymbol{J}_k$ and trial step $\boldsymbol{d}_k$ are computed, and the parameters for the subsequent iteration are derived as follows [19]:

$$\begin{cases} (\boldsymbol{J}_k^T\boldsymbol{J}_k + \lambda_k\boldsymbol{I})\boldsymbol{d}_k = -\boldsymbol{J}_k^T\boldsymbol{F}_k, \\ \boldsymbol{x}_{k+1} = \boldsymbol{x}_k + \boldsymbol{d}_k, \end{cases} \tag{18}$$

where $\lambda_k = \|\boldsymbol{F}_k\|^2$ denotes the L-M parameter. If the condition $\left\|\boldsymbol{J}_k^T\boldsymbol{F}_k\right\| \le 10^{-5}$ is satisfied, or k has reached its upper limit (set to 10), the iteration is terminated.

B. The Proposed Non-Unit Protection Method

The proposed protection method contains three steps. The details are introduced as follows:

1) Step 1: Protection Start-up Criterion: The protection start-up criterion is designed based on the 1-mode voltage absolute variation, which can be expressed as follows:

$$|\Delta u_1| > \varepsilon_1, \quad \varepsilon_1 = \mathrm{rel}_1 \cdot |\Delta u_1|_{\max}, \tag{19}$$

where Δu_1 denotes the 1-mode voltage variation, ε_1 refers to the threshold, rel_1 represents the reliability factor set as 1.2 [16]. Value $|\Delta u_1|_{\max}$ is the maximum system allowed variation $|\Delta u_1|$ due to the change of system operating mode, which is generally considered as 5% of rated voltage.

2) Step 2: Faulty Zone Identification Criterion: According to (15), the $u^*_{\mathrm{b1,ext}}$ under external faults is less or equal to $u^*_{\mathrm{b1,int}}$ of the internal fault. In addition, u^*_{b1} is independent of R_{f}, in contrast to u_{b1}. Therefore, u^*_{b1} is preferred to identify faulty zone using the criterion as follows:

$$\mathrm{intg\_}u^*_{\mathrm{b1}} = \sum_{n=1}^{N} u^*_{\mathrm{b1}}(n) > \varepsilon_2,\ \varepsilon_2 = \mathrm{rel}_2 \cdot \mathrm{intg\_}u^*_{\mathrm{b1,max}}, \quad (20)$$

where $\mathrm{intg\_}u^*_{\mathrm{b1}}$ denotes the summation of u^*_{b1}, n denotes the sampling order, N denotes the summation upper limit, which is set to 5 to guarantee both the detection speed and accuracy [16]. ε_2 denotes the threshold, $\mathrm{rel}_2 = 1.05$ denotes the reliability factor, and $\mathrm{intg\_}u^*_{\mathrm{b1,max}}$ denotes the integral of u^*_{b1} when F1 occurs at the cable end.

3) Step 3: Faulty Pole Identification Criterion: The criterion for pole identification is:

$$\begin{cases} \text{PPTG: } \mathrm{intg\_}u_0 < -\varepsilon_3, \\ \text{NPTG: } \mathrm{intg\_}u_0 > \varepsilon_3, \qquad \varepsilon_3 = \mathrm{rel}_3 \cdot |\mathrm{intg\_}u_0|_{\max}, \\ \text{PTP: } -\varepsilon_3 < \mathrm{intg\_}u_0 < \varepsilon_3, \end{cases} \quad (21)$$

where $\mathrm{intg\_}u_0 = \sum_{n=1}^{N} u_0(n)$ denotes the summation of 0-mode voltage summation, ε_3 denotes the threshold, and $\mathrm{rel}_3 = 1.2$ denotes the reliability factor. Similarly with $|\Delta u_1|_{\max}$ in (19), the $|\mathrm{intg\_}u_0|_{\max}$ refers to the maximum system allowed variation of $|\mathrm{intg\_}u_0|$.

C. Protection Working Principle

The flowchart of the proposed protection method, which consists of three steps, is shown in Fig. 3. To begin with, $|\Delta u_1|$ is calculated to determine whether the start-up criterion is met according to (19). If the protection is activated, it moves to the next step that fits the A of u_{b1} using the L-M algorithm and calculates the u^*_{b1} to identify the faulty zone according to (20). Once an internal fault is specified, the $\mathrm{intg\_}u_0$ is calculated to determine the specific faulty pole according to (21). Finally, the commands will be tripped to the corresponding DCCB for fault current interruption. Otherwise, the protection will be reset.

IV. Simulation and Verification

The MTDC system depicted in Fig.1 is simulated in PSCAD/EMTDC. All simulated faults are set at 0 ms and last for 100 ms, and the sampling frequency is 20 kHz. The thresholds ε_1, ε_2, and ε_3 in equations (19)-(21) are set to 0.04 p.u., 3.00 p.u., and 0.20 p.u., respectively.

Various fault scenarios are simulated to verify the proposed protection method. For internal faults F1, $R_{\mathrm{f}} \in \{0.01\,\Omega, 10\,\Omega\}$. While for external faults, $R_{\mathrm{f}} = 0.01\,\Omega$. The fault location l varies from 10% to 90% of the cable length. Simulated waveforms for metallic PPTG internal faults F1 occurring at different fault distances and metallic PTP external faults F2 and F3 are provided in Fig.4. As indicated, for the u^*_{b1} of F1, the arrival time is delayed, the amplitude attenuates, and the waveform turns smooth as the fault distance increases.

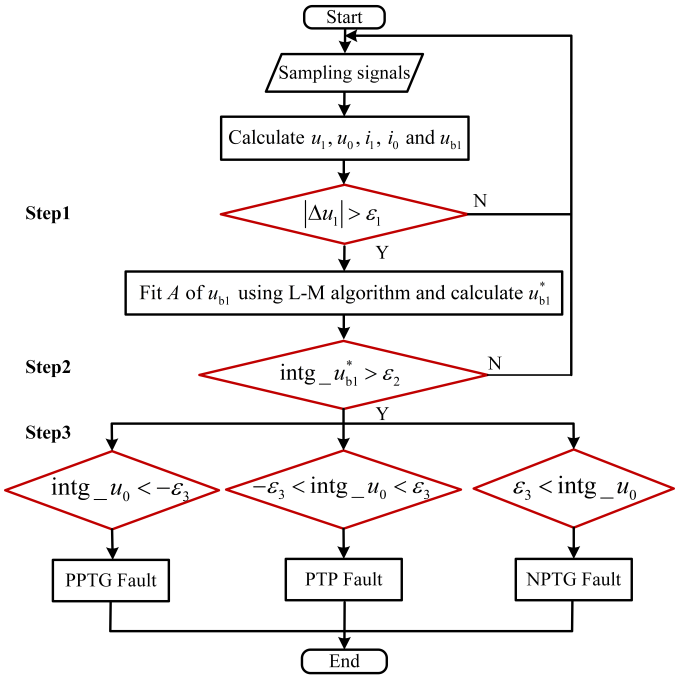

Fig. 3. The flowchart of the protection method.

Meanwhile, for the u^*_{b1} of F2 or F3, the aforementioned change are more intense, and the u^*_{b1} is less than F1, which is in alignment with the analysis in Section II.

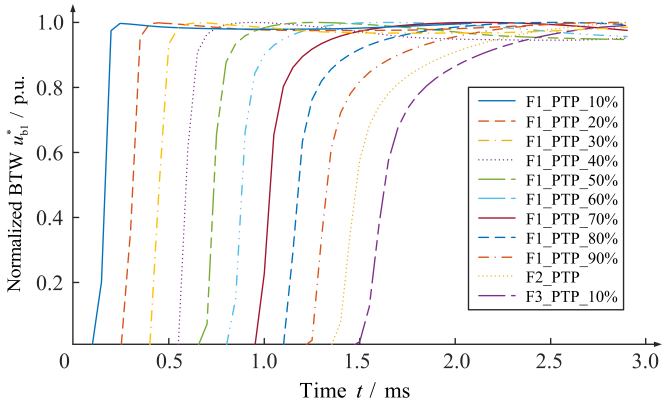

Fig. 4. The simulations of u^*_{b1} under different faults.

The results are shown in Table I. For all simulated scenarios, $|\Delta u_1|$ exceeds the threshold ε_1, satisfying the start-up criterion in (19), and the relays are activated. In the case of F1, the largest $\mathrm{intg\_}u^*_{\mathrm{b1}} = 4.55$ when a PTP metallic fault occurs with a small distance l. In contrast, the smallest $\mathrm{intg\_}u^*_{\mathrm{b1}} = 3.14$ when a PTP fault occurs with a long distance l and a large fault resistance R_{f}. Furthermore, the $\mathrm{intg\_}u_0$ under PPTG and PTP faults are distinctively different, allowing the correct selection of faulty poles. In contrast, when F2, F3, and F4 occur, criterion (20) is not satisfied, demonstrating the selectivity of the proposed method in identifying external faults.

Gaussian white noise (GWN) with a signal-to-noise ratio (SNR) of 35 dB is added to further analyze the robustness

of the proposed protection method. The results are shown in Table II. For all scenarios, the $|\Delta u_1|$ exceeds threshold ε_1, and the start-up criterion (19) can be satisfied correctly. It is seen that GWN has a random effect on $\mathrm{intg\_}u^*_{\mathrm{b}1}$, but it can be weakened by summation with a time window. Hence, the $\mathrm{intg\_}u^*_{\mathrm{b}1}$ is above the threshold ε_2 in all cases of F1, and the faulty zone is detected correctly. Similarly, $\mathrm{intg\_}u_0$ of PPTG or PTP faults can activate the criterion for faulty pole identification, respectively, even with noise interference. In contrast, the criterion (20) is not satisfied when F2, F3, and F4 occur, demonstrating the superior selectivity performance of the proposed method against the noise.

TABLE I
IDENTIFICATION RESULTS UNDER DIFFERENT SCENARIOS

Scenario	$R_{\mathrm{f}} = 0.01\ \Omega$			$R_{\mathrm{f}} = 10.0\ \Omega$		
	$\lvert\Delta u_1\rvert$	$\mathrm{intg\_}u^*_{\mathrm{b}1}$	$\mathrm{intg\_}u_0$	$\lvert\Delta u_1\rvert$	$\mathrm{intg\_}u^*_{\mathrm{b}1}$	$\mathrm{intg\_}u_0$
F1_PPTG_10%	0.46	4.55	-2.83	0.23	4.03	-1.53
F1_PPTG_50%	0.23	4.27	-1.72	0.11	3.57	-0.94
F1_PPTG_90%	0.10	3.42	-0.98	0.05	3.22	-0.60
F1_PTP_10%	0.93	4.28	-0.02	0.61	3.89	-0.01
F1_PTP_50%	0.46	4.10	0.01	0.30	3.83	-0.01
F1_PTP_90%	0.19	3.43	-0.01	0.12	3.14	0.01
F2_PTP	0.15	2.92	/	/	/	/
F3_PTP_10%	0.11	2.80	/	/	/	/
F4_PTP	0.97	0	/	/	/	/

TABLE II
IDENTIFICATION RESULTS WITH 35DB NOISE

Scenario	$R_{\mathrm{f}} = 0.01\ \Omega$			$R_{\mathrm{f}} = 10.0\ \Omega$		
	$\lvert\Delta u_1\rvert$	$\mathrm{intg\_}u^*_{\mathrm{b}1}$	$\mathrm{intg\_}u_0$	$\lvert\Delta u_1\rvert$	$\mathrm{intg\_}u^*_{\mathrm{b}1}$	$\mathrm{intg\_}u_0$
F1_PPTG_10%	0.46	4.34	-2.80	0.22	4.03	-1.47
F1_PPTG_50%	0.27	4.15	-2.11	0.14	3.74	-1.13
F1_PPTG_90%	0.18	3.45	-1.40	0.09	3.12	-0.97
F1_PTP_10%	0.85	4.33	-0.01	0.61	3.86	0.01
F1_PTP_50%	0.45	4.02	-0.01	0.32	3.90	-0.01
F1_PTP_90%	0.21	3.22	0.01	0.15	3.38	-0.01
F2_PTP	0.25	2.82	/	/	/	/
F3_PTP_10%	0.20	2.77	/	/	/	/
F4_PTP	0.91	0	/	/	/	/

V. CONCLUSION

DC line protection is essential for developing large-scale MTDC systems. This paper proposed a non-unit DC line protection method based on the normalized backward traveling waves of 1-mode voltage, and theoretical analysis and simulation verification conclude that:

1. When internal faults occur, the normalized backward traveling waves decrease as the distance increases. When external faults occur, none of their normalized backward traveling waves are greater than internal faults.

2. Levenberg-Marquardt algorithm is effective for fitting the amplitude of the backward traveling waves and thus calculating the normalized backward traveling waves.

3. The proposed protection method can correctly identify faults without boundary devices and is robust to noise. Furthermore, it has been verified that the method performance is unaffected by fault resistance, and the thresholds can be pre-set using analytical calculations.

REFERENCES

[1] A. Heidary, M. Popov, A. Moghim, M. G. Niasar, and A. Lekić, "The principles of controlled dc reactor fault current limiter for battery energy storage protection," *IEEE Transactions on Industrial Electronics*, pp. 1–9, 2023.

[2] L. Liu, A. Lekić, and M. Popov, "Robust adaptive back-stepping control approach using quadratic lyapunov functions for mmc-based hvdc digital twins," in *International Symposium on Leveraging Applications of Formal Methods*. Springer, 2022, pp. 126–138.

[3] L. Liu, A. Shetgaonkar, and A. Lekić, "Interoperability of classical and advanced controllers in mmc based mtdc power system," *International Journal of Electrical Power & Energy Systems*, vol. 148, p. 108980, 2023.

[4] W. Xiang, S. Yang, G. P. Adam, H. Zhang, W. Zuo, and J. Wen, "Dc fault protection algorithms of mmc-hvdc grids: Fault analysis, methodologies, experimental validations, and future trends," *IEEE Transactions on Power Electronics*, vol. 36, no. 10, pp. 11 245–11 264, 2021.

[5] L. Liu, Z. Liu, M. Popov, P. Palensky, and M. A. M. M. van der Meijden, "A fast protection of multi-terminal hvdc system based on transient signal detection," *IEEE Transactions on Power Delivery*, vol. 36, no. 1, pp. 43–51, 2021.

[6] N. Tong, X. Lin, Y. Li, Z. Hu, N. Jin, F. Wei, and Z. Li, "Local measurement-based ultra-high-speed main protection for long distance vsc-mtdc," *IEEE Transactions on Power Delivery*, vol. 34, no. 1, pp. 353–364, 2019.

[7] S. Li, W. Chen, X. Yin, D. Chen, and Y. Teng, "A novel integrated protection for vsc-hvdc transmission line based on current limiting reactor power," *IEEE Transactions on Power Delivery*, vol. 35, no. 1, pp. 226–233, 2020.

[8] J. Sun, S. Debnath, M. Bloch, and M. Saeedifard, "A hybrid dc fault primary protection algorithm for multi-terminal hvdc systems," *IEEE Transactions on Power Delivery*, vol. 37, no. 2, pp. 1285–1294, 2022.

[9] S. Zhang, G. Zou, C. Wang, J. Li, and B. Xu, "A non-unit boundary protection of dc line for mmc-mtdc grids," *International Journal of Electrical Power & Energy Systems*, vol. 116, p. 105538, 2020.

[10] J. Liu, N. Tai, and C. Fan, "Transient-voltage-based protection scheme for dc line faults in the multiterminal vsc-hvdc system," *IEEE Transactions on Power Delivery*, vol. 32, no. 3, pp. 1483–1494, 2017.

[11] N. Geddada, Y. M. Yeap, and A. Ukil, "Experimental validation of fault identification in vsc-based dc grid system," *IEEE Transactions on Industrial Electronics*, vol. 65, no. 6, pp. 4799–4809, 2018.

[12] B. Li, Y. Li, J. He, and W. Wen, "A novel single-ended transient-voltage-based protection strategy for flexible dc grid," *IEEE Transactions on Power Delivery*, vol. 34, no. 5, pp. 1925–1937, 2019.

[13] S. Liu, M. Popov, S. S. Mirhosseini, S. Nee, T. Modeer, L. Angquist, N. Belda, K. Koreman, and M. A. M. M. van der Meijden, "Modeling, experimental validation, and application of varc hvdc circuit breakers," *IEEE Transactions on Power Delivery*, vol. 35, no. 3, pp. 1515–1526, 2020.

[14] S. S. Mirhosseini, S. Jamali, and M. Popov, "Non-unit protection method for long transmission lines in mtdc grids," *IET Generation, Transmission & Distribution*, vol. 15, no. 11, pp. 1674–1687, 2021.

[15] C. Zhang, G. Song, and X. Dong, "A novel traveling wave protection method for dc transmission lines using current fitting," *IEEE Transactions on Power Delivery*, vol. 35, no. 6, pp. 2980–2991, 2020.

[16] L. Liu, A. Lekić, and M. Popov, "Robust traveling wave-based protection scheme for multiterminal dc grids," *IEEE Transactions on Power Delivery*, vol. 38, no. 5, pp. 3117–3129, 2023.

[17] R. Li, L. Xu, and L. Yao, "Dc fault detection and location in meshed multiterminal hvdc systems based on dc reactor voltage change rate," *IEEE Transactions on Power Delivery*, vol. 32, no. 3, pp. 1516–1526, 2017.

[18] L. Liu, F. Xie, M. Popov, Z. Hao, and A. Lekić, "Single-ended dc fault location method for mmc-based hvdc power system using adaptive multi-step levenberg-marquardt algorithm," in *2023 IEEE Belgrade PowerTech*, 2023, pp. 1–6.

[19] J. Fan, "The modified levenberg-marquardt method for nonlinear equations with cubic convergence," *Mathematics of Computation*, vol. 81, no. 277, pp. 447–466, 2012.